Optics Communications 494 (2021) 127041

Contents lists available at ScienceDirect

Optics Communications

journal homepage: www.elsevier.com/locate/optcom

Common path-based mobile free-space optical terminal with adaptive beamforming function for Gbps out-of-band full-duplex connectivity to UAVs

Siwoong Park [a,b], Chan Il Yeo [b], Young Soon Heo [b], Ji Hyoung Ryu [b], Hyun Seo Kang [b], Sung Chang Kim [b,*], Jae Hyung Jang [a,*]

[a] School of Electrical Engineering and Computer Science, Gwangju Institute of Science and Technology, 123 Cheomdangwagi-ro, Buk-gu, Gwangju, 61005, Republic of Korea

[b] Optical ICT Convergence Research Section, Honam Research Center, Electronics and Telecommunications Research Institute, 176-11 Cheomdangwagi-ro, Buk-gu, Gwangju, 61012, Republic of Korea

ARTICLE INFO

Keywords:
Free-space optics (FSO)
Beamforming
Full-duplex
Mobility
Unmanned aerial vehicle (UAV)

ABSTRACT

This paper presents simple and compact mobile free-space optical (FSO) terminals based on a common optical path with an adaptive beamforming function to provide an enhanced Gbps out-of-band full-duplex connection between a ground control system and an unmanned aerial vehicle (UAV). The mobile FSO terminals were carefully designed considering the UAV mobility and payload and the trade-off relationship between the geometric loss and volume of the FSO terminal for a given aperture diameter. Useful parameter information, such as the geometric loss, volume, and aperture diameter are presented in detail. As the novel common optical path structure-based mobile FSO terminal has a simple structure design and less optical components, it can effectively reduce the size, weight, and power consumption for UAV mounting. The beamforming function within the proposed system improves the optical tracking efficiency between FSO terminals by varying the divergence angle (from 0 to 8.84 mrad) according to the data link length. With the help of the beamforming function, the mobile FSO terminals showed significantly improved connectivity compared to the terminals employing collimated beams and fixed angle beams. Consequently, the proposed mobile FSO terminals provide reliable 1.25-Gbps out-of-band full-duplex error-free (with a bit error rate of $<10^{-12}$) connectivity. This study also presents an analysis of the geometric loss and volume corresponding to the size of the aperture diameter of the mobile FSO terminals for realizing high data rate out-of-band full-duplex FSO communication for flight platforms.

1. Introduction

With the growth of the application area and market of unmanned aerial vehicles (UAVs), the high data rate communication between UAVs and ground control systems (GCSs) is highly demanded [1–5]. Moreover, security and privacy concerns are emerging for UAV communication [3,4]. Free-space optical (FSO) systems are one of the best candidates for UAV communications thanks to its wide bandwidth and high level of security [1–5]. FSO communication is superior to conventional radio-frequency-based wireless communication in terms of low power consumption, directional and long-range propagation, and immunity to jamming and electromagnetic interference [1–12]. UAV-assisted FSO communication has recently attracted widespread attention with the aim of providing favorable solutions for fixed-to-fixed relay-assisted FSO networks and the backhaul/fronthaul of emerging 5G+ wireless networks. This is achieved owing to the flexible configuration and fast deployment and ability to provide better channel conditions [1,2,13,14]. In the realization of UAV-assisted FSO communication systems, the mobility of UAVs poses a crucial challenge for optical tracking techniques to establish a precise line-of-sight (LOS) link between a pair of mobile FSO terminals. It also impedes the dynamic system from controlling the beam divergence angle to provide sufficient signal energy to the receiver terminal regardless of the flight position of the UAVs (i.e., length of data link). The method of controlling the divergence angle is also useful for increasing the speed of optical tracking by widening the tracking beam. There are also important design considerations for mobile FSO terminals that are mounted on UAVs; these considerations are related to the weight and volume of the payload and the power consumption [2–5]. Moreover, mobile FSO terminals should be prepared for the degradation of UAV flight stability and FSO connectivity due to unwanted UAV fluctuations [15]. There have been limited studies on the implementation of UAV-assisted *out-of-band* full-duplex FSO communication systems that provide high

* Corresponding authors.
E-mail addresses: swp@etri.re.kr (S. Park), sungchang@etri.re.kr (S.C. Kim), jjang@gist.ac.kr (J.H. Jang).

https://doi.org/10.1016/j.optcom.2021.127041
Received 26 December 2020; Received in revised form 24 March 2021; Accepted 18 April 2021
Available online 24 April 2021

data rates (i.e., >1 Gbps), and even those studies are mostly theoretical [4,10]. Oxford University and the Airbus group also demonstrated a mobile FSO link using a drone equipped with a modulating retro-reflector (MRR) [4]. Unfortunately, this system can only provide a simplex connection from the drone to a GCS at a speed of 2 Mbps. The UAV-assisted high-capacity FSO link was recently demonstrated with a drone using orbital-angular-momentum multiplexing [10]. However, the drone only carried a lightweight retro-reflector (i.e., without carrying a transmitter or receiver for communication) to reflect and return the beam transmitted from a ground transmitter; essentially, the drone acted as a reflector. To accomplish UAV-assisted Gbps *out-of-band* full-duplex FSO links, UAVs must be equipped with mobile FSO terminals (i.e., compact and lightweight) with transceivers that can provide Gbps *out-of-band* full-duplex connection. In addition, practical guidelines are necessary to develop mobile FSO terminals more efficiently.

In this study, we propose a mobile FSO terminal with a simple structure based on a common optical path with an adaptive beamforming function to establish a reliable Gbps *out-of-band* full-duplex connection between a GCS and a UAV. The proposed FSO terminals share some of the optical and electrical components for beacon tracking and data communication with less optical components and a simple structural design. The beamforming function, which can effectively manage the beam divergence angle, automatically controls the signal intensity, which varies with the length of the data link between the FSO terminals, and improves the tracking speed and connectivity.

The remainder of this paper is organized as follows. Section 2 introduces the structure of an FSO terminal based on a common optical path, and analyzes the parameters to be considered when designing an FSO terminal, such as geometric loss, aperture diameter, length of data link, and divergence angle. In Section 3, the derived FSO terminals are evaluated by conducting optical simulations and preliminary experiments before field trials using a UAV. Finally, Section 4 concludes this work.

2. Design and experimental details

Fig. 1(a) presents the concept of our mobile FSO system that provides *out-of-band* full-duplex connectivity between a GCS and a UAV. Light sources of different wavelengths with the C-band (1530–1565 nm) and the L-band (1565–1625 nm) were utilized for *out-of-band* full-duplex data communication and beacon tracking. Fig. 1(b) shows the schematic diagram of the common path-based optical design for (i) the GCS terminal and (ii) the UAV terminal. As depicted in Fig. 1(b), the FSO terminal for the UAV was designed with a lower volume than that for the GCS. To reduce the number of optical and electrical components, volume, weight, power consumption, and manufacturing cost of the mobile FSO terminals, various optical components for data communication and beacon tracking were shared between the two terminals. A wavelength-division multiplexing (WDM) filter was employed to distinguish between the transmitting and receiving beams. A beam splitter (BS) was used to split the receiving beam toward an InGaAs-based 1.25-Gbps avalanche photodiode (APD) module and a p-i-n quadrant photodiode (QPD), at a ratio of 7:3, for the purpose of data communication and beacon tracking. The reason for this design is that mobile FSO terminals with separate optical beacon and data communication subsystems have many variables of misalignment. This is caused by the use of different lasers by optical beacon and data communication subsystems, resulting from the increase in the required components, such as the subdivision of the optical path due to the increase in the optical components, and the increase in the control elements of electrical components. Additionally, these systems face increased computational complexity and tracking loops owing to the structural complexity of each subsystem configuration and the several misalignment variables. Conversely, our design-based approach simplifies the tracking procedure for the data link compared to that of a mobile FSO terminal with separate optical beacon and data communication subsystems that require complex computations and tracking loops [4,5,16,17]. This is because our mobile FSO terminal splits the receiving beam for beacon tracking and data communication so that the establishment of the data link is concurrent with that of the beacon alignment. Therefore, our system eliminates these misalignment variables by driving the optical beacon subsystem and data communication subsystem using a single laser source with a simple common optical-path-based structure. Two different transmission wavelengths of 1530 nm (UAV terminal) and 1590 nm (GCS terminal) were used to minimize unwanted signal attenuation during propagation within the mobile FSO terminal and to prevent unwanted crosstalk due to internal reflection. Bandpass filters (BPFs) were also applied to block crosstalk and background light (i.e., sunlight). A motorized fiber stage including an output fiber, was employed to adjust the divergence angle of the transmission beam by changing the distance between the output fiber and WDM filter. It is a simpler beamforming method compared with other techniques utilizing a variable-focus liquid lens, movable lenses, a $1 \times N$ optical switch connected to the N output ports, or optical phase array antennas [18–20] (see Fig. 2).

The aperture diameter of the transmitter (Tx) and receiver (Rx) is one of the significant parameters determining the total volume of the FSO terminal and the receiving power. To determine the suitable aperture diameters for mobile FSO terminals, the geometric loss corresponding to the aperture diameter of a Tx and an Rx was investigated as a function of the length of the data link and beam divergence angle. Three different aperture diameters of 50, 70, and 100 mm were considered with reference to the previous reports on mobile FSO systems [4,5,16]. For simple calculations, we assumed that the received beam has a uniform power distribution at the Rx aperture. This is a valid assumption because the difference between a Gaussian power distribution and a uniform power distribution is very small if the diameter of the transmitted beam, which increases with the length of the data link, is several times larger than the Rx aperture. Geometric loss can be calculated using the following formula [21]:

$$Geometric\ loss\ (\mathrm{dB}) = 20log\left[D_R/\left(D_T + L \times \theta_{div}\right)\right], \quad (1)$$

where D_R is the diameter of the Rx aperture, D_T is the diameter of the Tx aperture, L is the length of the data link, and θ_{div} is the divergence angle. The units of the length and angle are meters and radians, respectively. As L and θ_{div} increase, the geometric loss increases significantly because the beam diameter is enlarged rapidly with the R_X aperture. From the calculation results, it can be inferred that a large R_X aperture diameter is required to reduce the geometric loss. It is necessary to carefully select the aperture diameter of the mobile FSO terminals, particularly for UAVs owing to the trade-off relationship between the geometric loss and *outer* volume (weight) of FSO terminals. *T*he volume and receiving power were calculated based on the aperture diameter in order to determine the optimal aperture diameter for the UAV terminal. An aperture with a diameter of 100 mm, exhibiting a relatively low geometric loss, was utilized for the GCS terminal with a less stringent weight limitation.

Fig. 3(a) presents a schematic diagram of the FSO terminal for a UAV in order to evaluate the volume and receiving power as a function of the aperture diameter. For the practical system design, the electrical components that are required to operate the mobile FSO terminal and manual stages for alignment of the various optical components are included. An erbium-doped fiber amplifier (EDFA) was integrated to obtain the optical gain. For *out-of-band* full-duplex data transmission, an Ethernet fiber network card was integrated. As shown in the inset of Fig. 3(a), a programmable motorized fiber stage (mightyZAP L12-12F-3, IR ROBOT Co.) with a small form factor was integrated to control the beam divergence angle. It is important to note that the precise alignment of the mechanical axis of the motorized fiber stage and the optical axes of the output fiber and lens system is essential to prevent unwanted displacement of the transmitted beam at the receiver terminal. The optical and mechanical axes can be easily aligned by

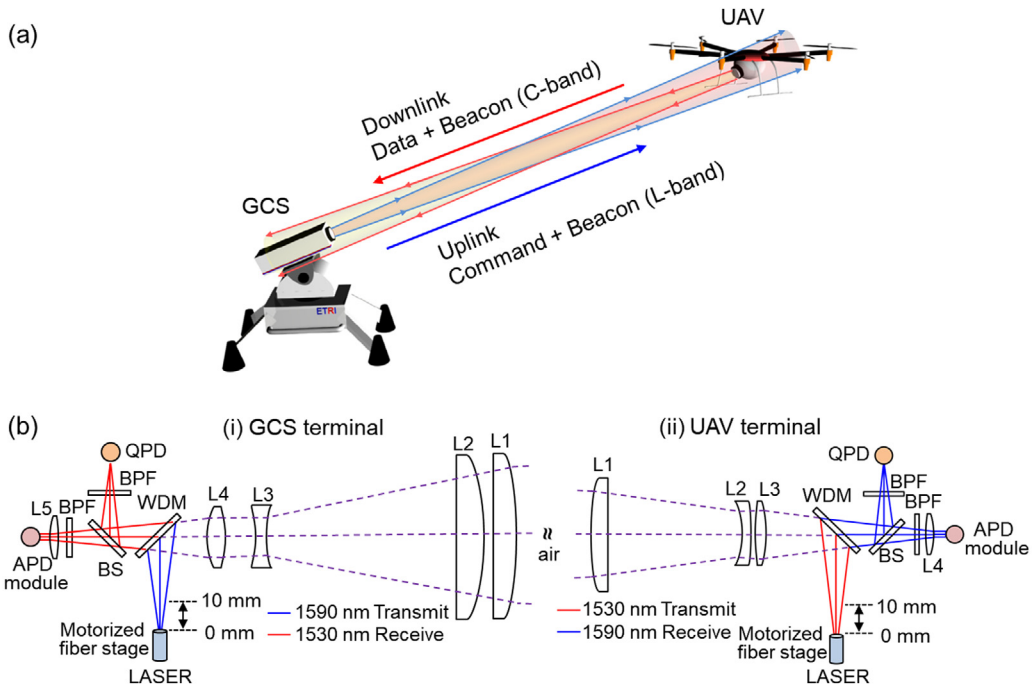

Fig. 1. (a) Graphic of our target mobile free-space optical (FSO) system between a ground control system (GCS) and an unmanned aerial vehicle (UAV). (b) Schematics of the optical design for (i) GCS terminal and (ii) UAV terminal.

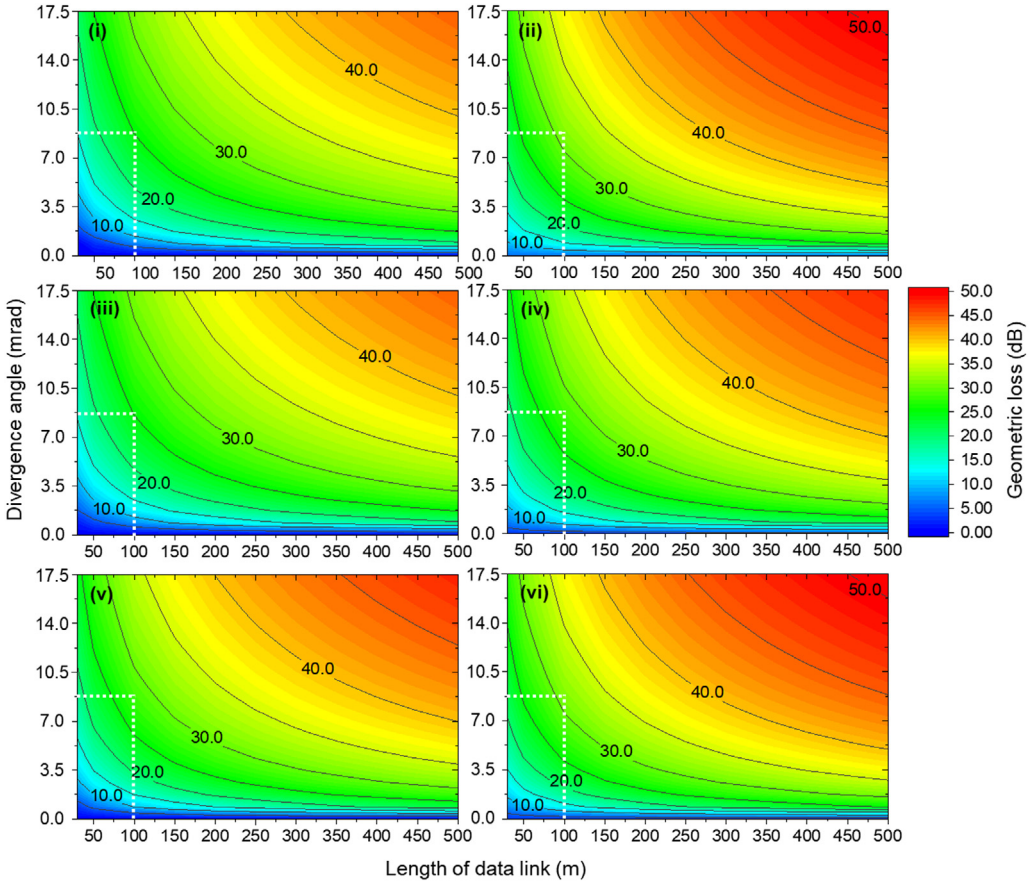

Fig. 2. Contour plots of calculated geometric loss depending on the length of data link and the divergence angle corresponding to aperture diameters for transmitter (Tx)-to-receiver (Rx) of (i) 50-to-100 mm, (ii) 100-to-50 mm, (iii) 70-to-100 mm, (iv) 100-to-70 mm, (v) 50-to-70 mm, and (vi) 70-to-50 mm.

moving the motorized fiber stage back and forth and monitoring the center position of the incident beam using an iris diaphragm and a beam viewer (BeamMaster BM-3 InGaAs, Coherent Inc.). It is essential that the center of gravity (CoG) of the mobile FSO terminal and the

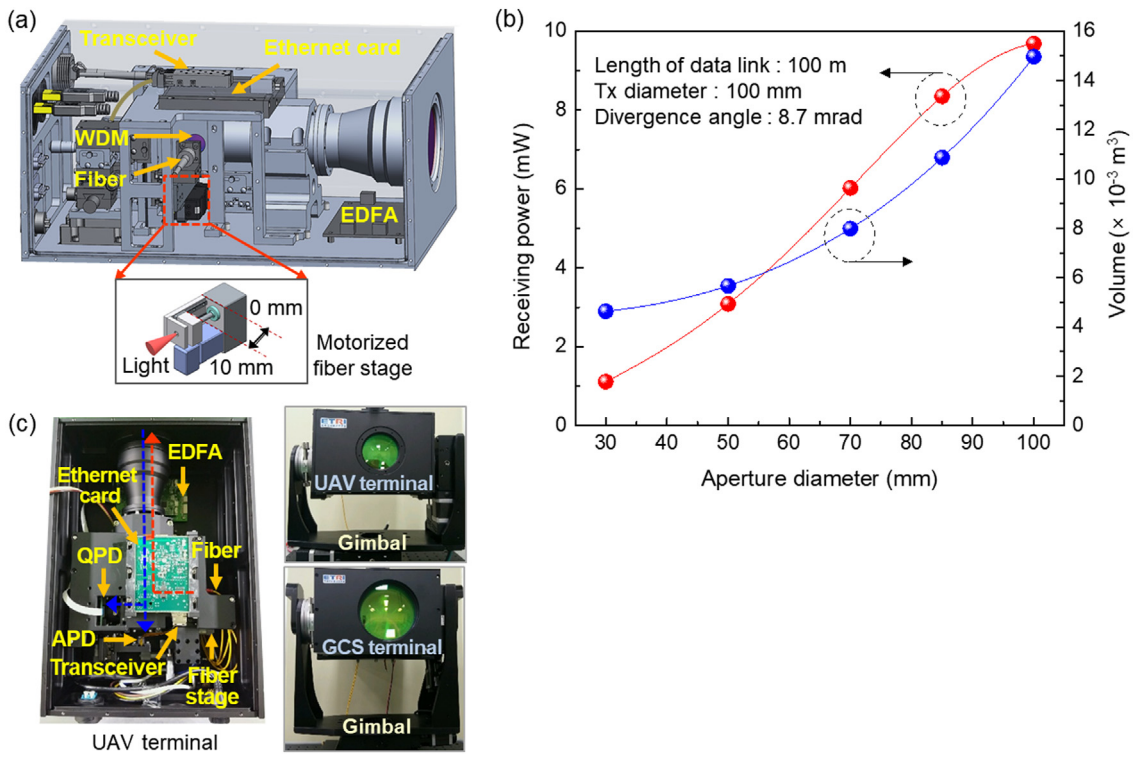

Fig. 3. (a) Schematic diagram of the mobile FSO terminal for UAV. (b) Calculated receiving power and volume of the mobile FSO terminal for UAV as a function of aperture diameter. (c) Photographs of the prototype terminals for GCS and UAV.

gimbal axis of the UAV match to suppress the fluctuation and sway of the UAV. Therefore, the optical and electrical components were matched to those of the CoG of the FSO terminal and the gimbal axis of the UAV. Fig. 3(b) shows the calculated optical power incident to the R_X aperture when the length of the data link and divergence angle are fixed at 100 m and 8.7 mrad, respectively. It also shows the estimated volume of individually designed FSO terminals with respect to the aperture diameter. *Because the length the terminal depends on the enclosed optical components and electronics and the sidewall area where the optical aperture is placed depends on the aperture diameter, the outer volume of the terminal quadratically increases with the aperture diameter.*

The LightTools simulator was used for optical simulations, and the light sources used in the simulation had a power output of 200 mW and a Gaussian beam profile. From Fig. 3(b), it is observed that the volume decreases slowly, but the receiving power decreases at a constant rate when the aperture diameter is smaller than 70 mm. This occurs because the major factor determining the volume of the FSO terminal changes from the aperture diameter to the electrical components and manual stages when the aperture diameter decreases below 70 mm. The appropriate aperture diameter for the UAV terminal was to approximately 70 mm considering that the ratio of the received power over the volume is maximized at an aperture diameter of 70 mm. Fig. 3(c) shows the prototypes of the mobile FSO terminal for the UAV and GCS. The total weight of the prototype terminals is less than 8 and 12 kg for the UAV and GCS, respectively. In the preliminary experiments, the prototypes were mounted onto a gimbal whose *maximum angular velocity is* 0.7 rad/s. *For the* 90-m-*long FSO link, the maximum UAV speed supported by the gimbal system is* 75.5 m/s. LOS between the mobile FSO terminals was accomplished with the help of our QPD sensor-based active alignment [11]. *A global positioning system (GPS) signals for cross-terminal heading and searching are also utilized for the tracking to cope with the optical channel block. This hybrid tracking methods enables fast LOS channel recovery.* Most of the simulations and experiments were carried out using the mobile FSO terminal designed for the UAV as a Tx and the other terminal as a Rx because, herein, the focus is primarily on the dynamic movement of the UAVs rather than the stationary GCS.

Prior to conducting the experiments, optical simulations were carried out to investigate the transmitted beam profile at the Rx terminal corresponding to the length of the data link and position of the output fiber (i.e., beam divergence angle). Fig. 4(a) shows the calculated beam profile, peak intensity, and beam diameter at the Rx terminal as a function of the length of the data link. In the calculations, the position of the output fiber was fixed at 10 mm. As the length of the data link increased, the peak intensity decreased drastically owing to the increased geometric loss [21]. In order to provide sufficient signal energy to the corresponding FSO terminal, adaptive beamforming that can control the beam divergence angle corresponding to the length of the data link is indispensable in the mobile FSO system. Fig. 4(b) shows the calculated beam profile and peak intensity at the Rx terminal and the beam divergence angle corresponding to the position of the output fiber when the length of the data link is 90 m. As the position of the output fiber changes from 0 to 10 mm, the divergence angle varies linearly (0.673 mrad/mm) and the peak intensity drastically decreases. The abrupt change in the peak intensity is due to the geometric loss that is proportional to θ_{div}^2 [21]. It is found that the signal intensity at the Rx terminal can be easily controlled by adjusting the position of the output fiber. With the help of the motorized fiber stage, our mobile FSO system can be programmed to provide a predetermined signal energy to the Rx terminal according to the distance between a pair of mobile FSO terminals.

3. Results and discussion

Unwanted link failure in the mobile FSO systems can occur owing to unavoidable UAV vibrations and sway. Therefore, it is necessary to have a wide range of the rotatable angle (θ_{FR}) to maintain the data link without pointing errors and to suppress link failure and errors in the mobile FSO system. The θ_{FR} of the UAV terminal, within which error-free (BER $<10^{-12}$) *link is guaranteed, was calculated and measured for various beam divergence angles, and the variable length of the data link.* Fig. 5(a) shows the calculation results of the total receiving power

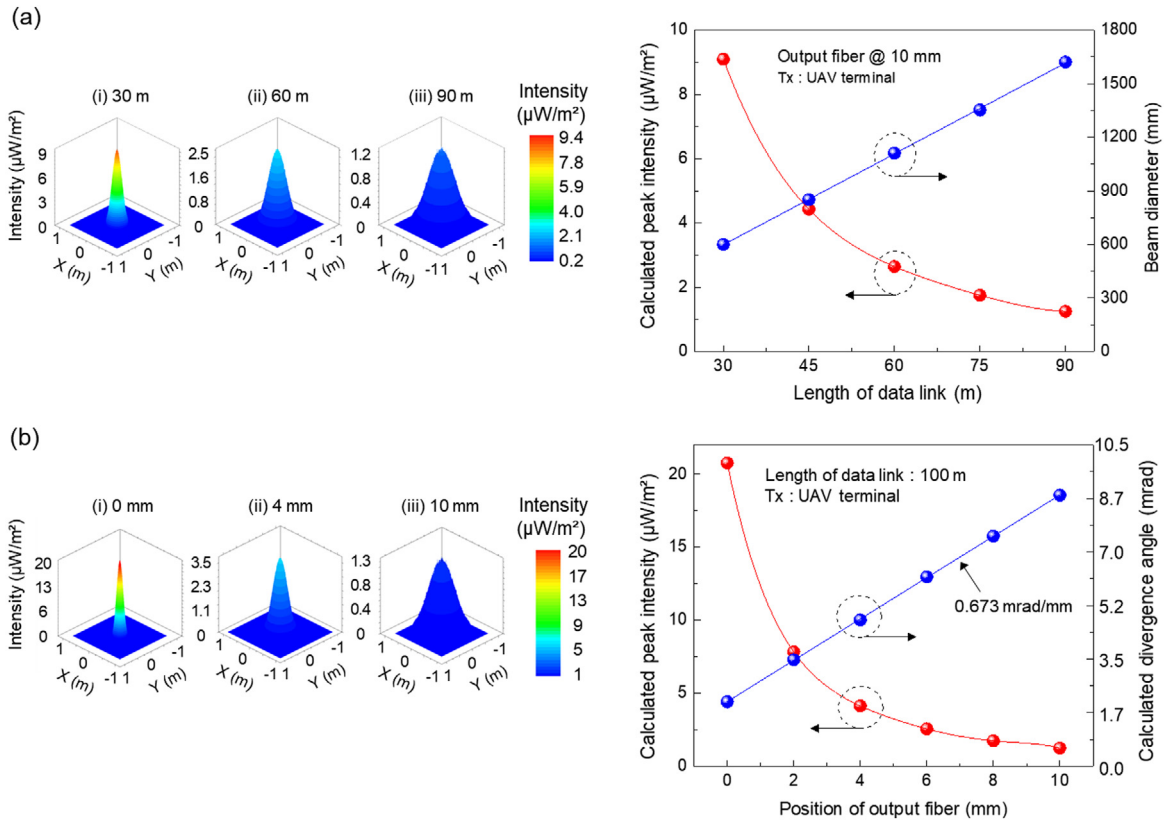

Fig. 4. (a) Calculated beam profile and diameter at the Rx terminal corresponding to the length of data link. (b) Calculated beam profile at the Rx terminal and divergence angle (θ_{div}) as a function of the position of output fiber.

by the APD and θ_{FR} corresponding to the position of the output fiber and the length of the data link. As the output fiber varies from 0 to 10 mm, θ_{FR} linearly increases, and the receiving power rapidly decreases owing to the significant increase in the geometric loss as the beam divergence angle increases. *When minimum beam divergence angle and the highest transmitter power* (200 mW) *are utilized, the error free link can be established up to* 13.6 km. *As the transmitter power is reduced to* 100 *and* 50 mW, *the maximum length of the error free link is reduced down to* 5.9 km *and* 3.4 km, *respectively. When the maximum divergence angle is employed, the extra power loss reduces the maximum link length down to* 1.2 km *even at the maximum transmitter power of* 200 mW. *To avoid link performance degradation, it is essential to utilize the adaptive beam narrowing strategy after the LOS link is established.*

The atmospheric absorption and scattering effects were not considered in the calculations for simplicity. Fig. 5(b) shows the measured power at the receiver and θ_{FR} as a function of the position of the output fiber for various data link lengths. As shown in Fig. 5(b), the overall behavior of the measured power at the receiver and θ_{FR} are consistent with the calculation results. This experimental result clearly shows that θ_{FR} can be effectively improved by increasing the beam divergence angle. Meanwhile, the minor decrease in θ_{FR} with the increase in the length of data link can be attributed to the decrease in the signal energy at the Rx terminal due to the absorption and scattering losses by the aerosol particles in the atmosphere [6]. Owing to the improved θ_{FR}, the connectivity of the mobile FSO system can be enhanced compared to those of collimated beams and fixed angle beams. This is because a large beam improves the tolerance to misalignment [2,3].

By employing large divergence angle at the transmitter, the beam diameter at the receiver can be increased and the scanning efficiency can be improved. The speed-up factor [4] has been defined to be the ratio between the beam size at the Rx FSO terminal at a certain divergence angle and the collimated beam size. Compared with the collimated beam size for a data link length of 90 m, the speed-up factor corresponding to the divergence angles obtained by positioning the output fiber at 0 mm and 10 mm were 2.2 and 16.7, respectively. When the larger beam diameter is employed to scan the target FSO terminal, the target detection probability can be increased [22]. *The measurement result of the*90-m-*long data link in Fig.* 5*(b) confirmed that the measured* θ_{FR} *at the maximum beam divergence angle (output fiber at* 10 mm*) was 2.32 times larger than that at the minimum beam divergence angle (output fiber at* 0 mm*). It is obvious that the beam with the larger divergence angle functions better than the collimated Gaussian beam having nearly zero divergence angle for scanning the target FSO terminal.* Alternatively, in case of poor weather conditions or high propagation losses, the beam divergence angle must be reduced to maintain the received power of the R_X terminal [6,7,9]. Accordingly, the programmable adaptive beamforming function is crucial for the practical application of mobile FSO systems. Fig. 5(c) and (d) show the calculated intensity charts at the APD and QPD of the Rx terminal, respectively, for various rotation angles (θ_R) of the UAV terminal. In the calculations, the length of the data link and the position of the output fiber were fixed at 90 m and 10 mm, respectively. As θ_R increases, the peak intensity and total received power of the APD and the QPD decrease mainly owing to the reduction of the signal energy incident to the aperture of the Rx terminal. As the θ_R of the Tx terminal increases, the optical intensity distribution on the QPD leans to one side, and eventually, the overlapped area is reduced. The QPD is essential to precisely detect the movement of the Tx and Rx terminals by calculating the normalized position of the incident beam on the QPD [23]. The active diameters of the APD and QPD used in this experiment were 0.2 mm and 3 mm, respectively. For mobile FSO links, it is important to note that an APD with a large absorption area is preferable for increasing the angle of arrival (AoA) and making the mobile FSO system robust to AoA fluctuations [15]. However, as the active area of the APD increases, its bandwidth decreases owing to the increased junction capacitance [24,25]. Hence, the APD should be chosen carefully, while

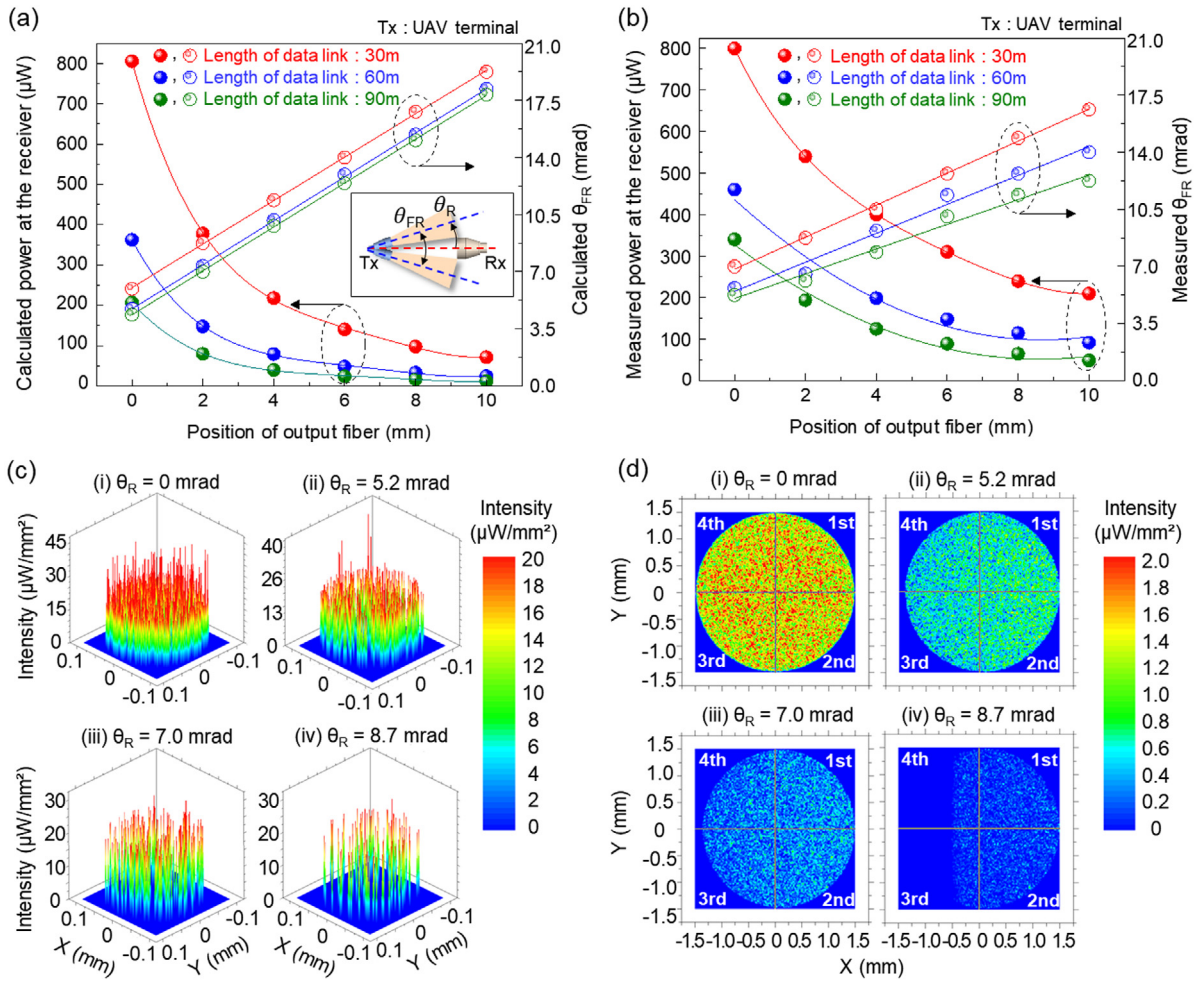

Fig. 5. (a) Calculated power at the receiver and θ_{FR}, and (b) measured power at the receiver and θ_{FR} as a function of the position of output fiber corresponding to the length of data link. Calculated intensity charts of (c) avalanche photodiode (APD) and (d) quadrant photodiode (QPD) according to the θ_R of Tx at the length of data link of 90 m and the output fiber of 10 mm.

designing the mobile FSO terminals, considering the target data rate and AoA requirements. The bit error rate (BER) performance was measured to investigate the quality of the FSO link that was established using the prototypes designed to provide a 1.25 Gbps *out-of-band* full-duplex data link. Fig. 6(a) illustrates the experimental setup to measure the BER performance of the 90-m-long mobile FSO link. The BER performance as a function of the beam divergence angle and the length of the data link was also investigated. Fig. 6(b) shows the measured θ_{FR} to achieve an error-free FSO link without forward error correction (FEC) corresponding to the position of the output fiber and length of the data link. As the position of the output fiber moves from 0 to 10 mm, θ_{FR} for an error-free FSO link also increases by more than 150% over the entire length of the data link. It is possible to further increase θ_{FR} by moving the output fiber further toward the WDM filter. The measured θ_{FR} used to achieve an error-free FSO link corresponding to the length of the data link is useful for the development of a custom-designed tracking algorithm and operational strategy for our mobile FSO system. Besides, achieving a stable and robust mobile FSO link between GCSs and UAVs requires a large θ_{FR} to acquire an error-free FSO link. A 1.25-Gbps pseudorandom data stream (2^7–1) using a non-return-to-zero scheme was utilized, and a Gigabit Ethernet mask pattern (light gray hexagonal pattern) with 40% margin (dark gray hexagonal pattern) was employed. The measured emission power and extinction ratio at the output fiber of the Tx terminal were approximately 23.1 dBm and 10 dB, respectively. Fig. 6(c) and (d) show the measured eye-diagram of a well-aligned error-free link with a BER of $<10^{-12}$ and a slightly misaligned link (i.e., error begin to occur) with a BER of $>9.5 \times 10^{-12}$, respectively. When the measured APD photocurrent was approximately 16.5 μA, the FSO link exhibited a BER of 9.5×10^{-12} without FEC. The FSO link does not guarantee error-free communication as the APD photocurrent drops below 16.5 μA.

An outdoor test was also carried out to measure the data throughput using a standard file transfer protocol (FTP) between a client and a server. Fig. 7(a) shows the experimental setup for the measurement of the data throughput of an *out-of-band* full-duplex transmission at a data link length longer than 100 m under clear weather conditions (34°C). In this experiment, a Gigabit Ethernet fiber network card with a 1000-Mbps Ethernet port acting as a 1000-Mbps client/server and an uncompressed 4K-resolution video file were utilized. Fig. 7(b) presents the measured data throughput of the *out-of-band* full-duplex transmission between a server (UAV terminal) and a client (GCS terminal) using an FTP. The measured average data throughput was 887.6 Mbps, and the maximum data throughput was 904.8 Mbps.

Several mobile FSO systems have been developed for various flight platforms, including drones, aircrafts, and balloons. Table 1 presents a summary of the representative mobile FSO systems based on flight platforms. MRR-based mobile FSO systems have been widely explored for flight platforms. This approach is advantageous because of the small volume, minimal weight, and easy implementation. However, the data rate and link range (R) are considerably limited by the low modulation speed of the MRR and the length of the data link (proportional to R^4), respectively [4,5]. Mobile FSO systems with separated optical paths for

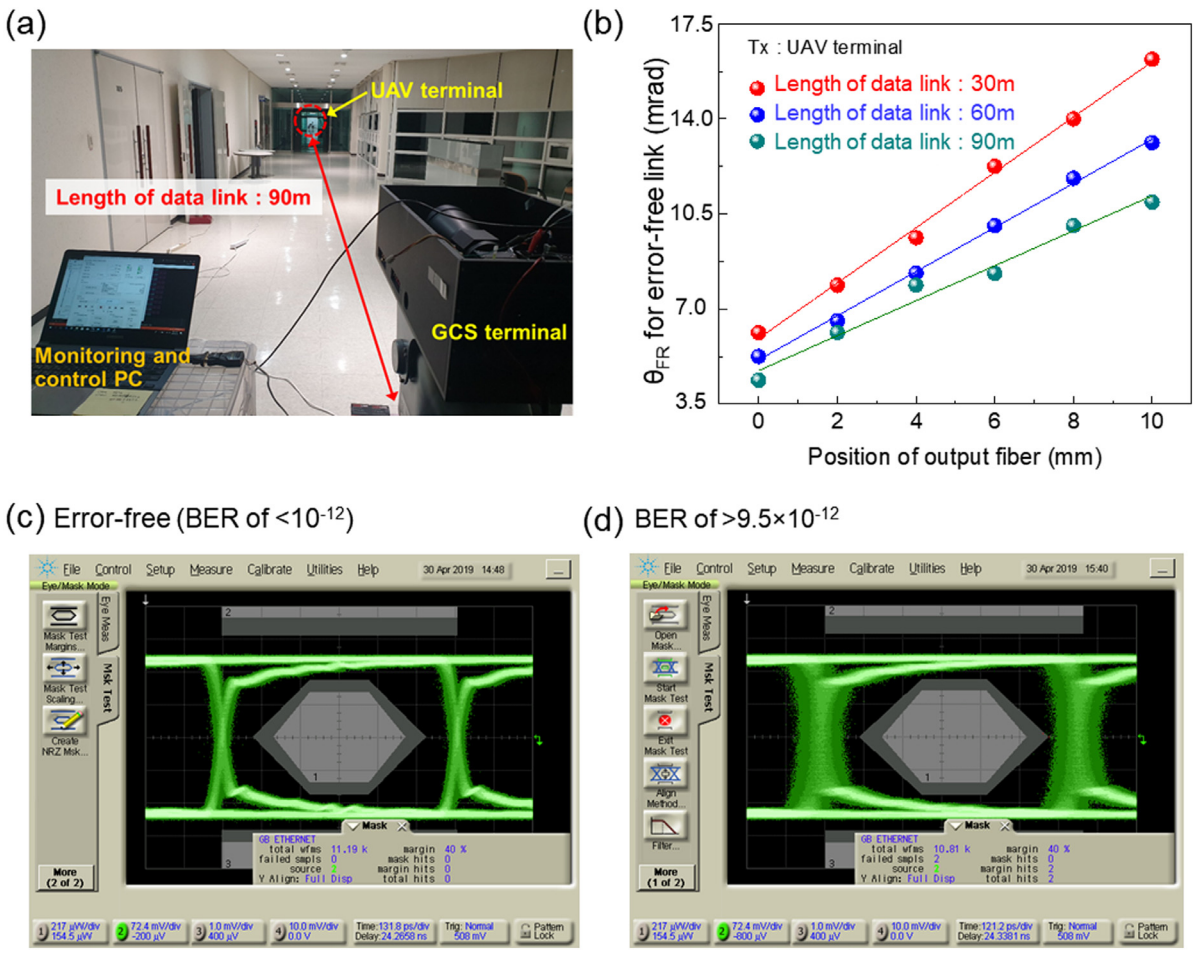

Fig. 6. (a) Experimental setup to measure bit error rate (BER) performance of the 90-m-long data link. (b) Measured θ_{FR} for an error-free FSO link as a function of the position of output fiber corresponding to the length of data link. Measured eye-diagrams of (c) an error-free (BER $<10^{-12}$) and (d) a BER of $>9.5 \times 10^{-12}$ FSO link.

Table 1
Mobile FSO systems for flight platforms.

Type of data transmission	Type of Tx/Rx	Optical path for Tx/Rx/Beacon	Link rate (Gbps)	Beamforming (θ_{div})	Number of optical components	Ref.
Simplex (Drone-to-Ground)	MRR/ Photodetector	Separate	0.002	SLM	15 (Ground)	[4]
Half-duplex (UAV-GCS)	MRR/ Photodetector	Separate	0.002	Fixed (300 μ rad)	–	[5]
Simplex (Airborne-to-Ground)	MLT/TOGS	Separate	1.25	Fixed (2.26 mrad)	≥ 23 (TOGS)	[26]
Full-duplex (Inter-Balloons)	Transceiver	Share	0.13	Fixed (280 μ rad)	–	[16]
Full-duplex (UAV-GCS)	Transceiver	Share	1.25	Auto-stage (0~8.84 mrad)	≤ 9 (GCS)	This work

SLM: spatial light modulation, MLT: micro laser terminal, TOGS: transportable optical ground station.

data communication and beacon tracking have been comprehensively explored [4,5,26]. However, separated optical paths are undesirable for use in mobile FSO systems because of the number of optical and electrical components and the volume, weight, and production cost of the FSO terminal. For flight platforms, an adaptive beamforming function can play an important role in improving FSO connectivity and enhancing the performance of the tracking system [4,24]. Our mobile FSO terminal exhibited a wide range of beam divergence angles (from 0 to 8.84 mrad), which are advantageous for both short and long-range FSO communication. Based on these points, we believe that our mobile FSO system can be deployed to realize high data rate mobile FSO communication systems and networks, which can be utilized by flight platforms.

4. Conclusion

Herein, common path-based Gbps *out-of-band* full-duplex mobile FSO terminals with an adaptive beamforming function were proposed to improve UAV connectivity. To realize the mobile FSO system for UAVs, we carefully considered important issues such as the mobility and payload of the UAVs, and provided practical guidelines and useful information. Particularly, we analyzed the geometric loss and volume corresponding to the size of the aperture diameter. Further, we estimated the beam intensity and rotatable angle, which vary with the changes in the beamforming function-based divergence angle, to maintain a robust data link connectivity, *which improves the optical tracking*

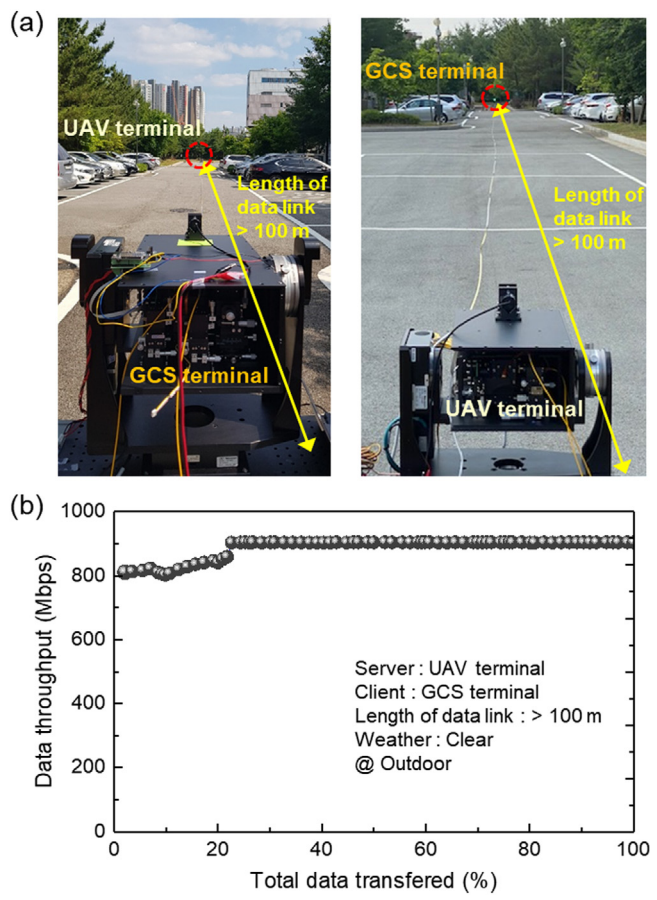

Fig. 7. (a) Experimental setup for outdoor testing over the 100-m-long data link. (b) Data throughput of *out-of-band* full-duplex transmission measured using file transfer protocol (FTP).

efficiency between FSO terminals. The estimated beam intensity and rotatable angle facilitate the efficient development of high-speed mobile FSO terminals. Moreover, we developed common optical-path-based FSO terminals with a simple structural design, less optical components, and reduced size, power consumption, and misalignment factors. The mobile FSO terminals showed great potential to providing a reliable 1.25-Gbps 90-m-long FSO link with a BER of $<10^{-12}$ and exhibited good performance in *out-of-band* full-duplex data transmission. The mobile FSO terminals also showed significantly improved connectivity, with a speed-up factor ranging from 2.2 to 16.7. The overall performance of our mobile FSO system confirms that it is competitive for small size, lightweight, low power consumption, and Gbps *out-of-band* full-duplex error-free connectivity being mounted on flight platforms in dynamic environments with varying data link lengths. *However, the impact of the atmospheric conditions and unwanted UAV vibrations on the link performance should be analyzed before the FSO terminal presented in this study to be used in real ground-UAV data links. More experimental works are required to this end.*

Declaration of competing interest

The authors declare that they have no known competing financial interests or personal relationships that could have appeared to influence the work reported in this paper.

Acknowledgments

Funding

This work was supported by Electronics and Telecommunications Research Institute (ETRI) grant funded by the Korean government [21ZK1100, Honam Region Regional Industry-based ICT Convergence Technology Advancement Support Project].

References

[1] W. Fawaz, C.A. Rjeily, C. Assi, UAV-aided cooperation for FSO communication systems, IEEE Commun. Mag. 56 (1) (2018) 70–75.
[2] Y. Dong, Z. Hassan, J. Cheng, J. Hossain, V.C.M. Leung, An edge computing empowered radio access network with UAV-mounted FSO fronthaul and backhaul: Key challenges and approaches, IEEE Wirel. Commun. 25 (3) (2018) 154–160.
[3] A. Kaadan, H.H. Refai, P.G. LoPresti, Multielement FSO transceivers alignment for inter-UAV communications, J. Lightwave Technol. 32 (24) (2014) 4785–4795.
[4] C. Quintana, G. Erry, A. Gomez, Y. Thueux, G.E. Faulkner, D.C. O'Brien, Design of a holographic tracking module for long-range retroreflector free-space systems, Appl. Opt. 55 (25) (2016) 7173–7178.
[5] W.S. Rabinovich, C.I. Moore, R. Mahon, P.G. Goetz, H.R. Burris, M.S. Ferraro, J.L. Murphy, L.M. Thomas, G.C. Gilbreath, M. Vilcheck, M.R. Suite, Free-space optical communications research and demonstrations at the U.S. Naval Research Laboratory, Appl. Opt. 54 (31) (2015) F189–F200.
[6] H. Kaushal, G. Kaddoum, Optical communication in space: Challenges and mitigation techniques, IEEE Commun. Surv. Tutor. 19 (1) (2017) 57–96.
[7] C.A. Rjeily, G. Kaddoum, G.K. Karagiannidis, Ground-to-air FSO communications: when high data rate communication meets efficient energy harvesting with simple designs, Opt. Express 27 (23) (2019) 34079–34092.
[8] Q. Huang, D. Liu, Y. Chen, Y. Wang, J. Tan, W. Chen, J. Liu, N. Zhu, Secure free-space optical communication system based on data fgmentation multipath transmission technology, Opt. Express 26 (10) (2018) 13536–13542.
[9] W.G. Alheadary, K.H. Park, N. Alfaraj, Y. Guo, E. Stegenburgs, T.K. Ng, B.S. Ooi, M.S. Alouini, Free-space optical channel characterization and experimental validation in a coastal environment, Opt. Express 26 (6) (2018) 6614–6628.
[10] L. Li, R. Zhang, Z. Zhao, G. Xie P. Liao, K. Pang, H. Song, C. Liu, Y. Ren, G. Labroille, P. Jian, D. Starodubov, B. Lynn, R. Bock, M. Tur, A.E. Willner, High-capacity free-space optical communications between a ground transmitter and a ground receiver via a UAV using multiplexing of multiple orbital-angular-momentum beams, Sci. Rep. 7 (17427) (2017) 1–12.
[11] J.H. Ryu, S.C. Kim, J.R. Ryoo, S.Y. Yi, Tracking control for free-space optical communication of unmanned aerial vehicle, in: 2018 IEEE 3rd International Conference on Communication and Information Systems, ICCIS, 2018, pp. 132–136.
[12] M.I. Petkovic, G.T. Djordjevic, Impact of temporary link blockage on ergodic capacity of FSO system, ETRI J. 40 (3) (2018) 330–336.
[13] M. Alzenad, M.Z. Shakir, H. Yanikomeroglu, M.S. Alouini, FSO-based vertical backhaul/fronthaul fmework for 5G+ wireless networks, IEEE Commun. Mag. 56 (1) (2018) 218–224.
[14] B. Yan, H. Liu, C. Li, X. Jiang, X. Li, J. Hou, H. Zhang, W. Lin, J. Liu, Laser-filamentation-assisted 1.25 Gb/s video communication under harsh conditions, Opt. Laser. Technol. 131 (2020) 106391.
[15] M.T. Dabiri, S.M.S. Sadough, M.A. Khalighi, Channel modeling and parameter optimization for hovering UAV-based free-space optical links, IEEE J. Sel. Areas Commun. 36 (9) (2018) 2104–2113.
[16] B. Moision, B. Erkmen, E. Keyes, T. Belt, O. Bowen, D. Brinkley, P. Csonka, M. Eglington, A. Kazmierski, N.H. Kim, J. Moody, T. Tu, W. Vermeer, Demonstration of free-space optical communication for long-range data links between balloons on Project Loon, Proc. SPIE 10096 (2017).
[17] A.C. Casado, R. Vergaz, J.M.S. Pena, In-axis reception by polarization discrimination in a modulating-retroreflector-based free-space optical communication link, Microw. Opt. Technol. Lett. 54 (11) (2012) 2520–2522.
[18] A. Joshi, J. Rue, S. Datta, Low-noise large-area quad photodetectors based on low-capacitance quad InGaAs photodiodes, IEEE Photonics Technol. Lett. 21 (21) (2009) 1585–1587.
[19] H. Ren, S.T. Wu, Variable-focus liquid lens, Opt. Express 15 (10) (2007) 5931–5936.
[20] K.H. Heng, W.D. Zhong, T.H. Cheng, N. Liu, Y. He, Beam divergence changing mechanism for short-range inter-unmanned aerial vehicle optical communications, Appl. Opt. 48 (8) (2009) 1565–1572.
[21] S. Bloom, E. Korevaar, J. Schuster, H. Willebrand, Understanding the performance of free-space optics, J. Opt. Netw. 2 (6) (2003) 178–200.
[22] X. Liu, Y. Yang, C. Ma, J. Li, S. Zhang, Real-time visual tracking of moving targets using a low-cost unmanned aerial vehicle with a 3-axis stabilized gimbal system, Appl. Sci. 10 (5064) (2020) 1–29.
[23] H. Kaushal, V.K. Jain, S. Kar, Acquisition, tracking, and pointing, in: Free Space Optical Communication, Springer, 2017.

[24] H. Kaushal, V.K. Jain, S. Kar, Free-space optical channel models, in: Free Space Optical Communication, Springer, 2017.
[25] A. Novack, M. Gould, Y. Yang, Z. Xuan, M. Streshinsky, Y. Liu, G. Capellini, A.E.J. Lim, G.Q. Lo, T.B. Jones, M. Hochberg, Germanium photodetector with 60 GHz bandwidth using inductive gain peaking, Opt. Express 21 (23) (2013) 28387–28393.
[26] F. Moll, J. Horwath, A. Shrestha, M. Brechtelsbauer, C. Fuchs, L.A.M. Navajas, A.M.L. Souto, D.D. González, Demonstration of high-rete laser communications from a fast airborne platform, IEEE J. Sel. Areas Commun. 33 (9) (2015) 1985–1995.